DOI: 10.13009/EUCASS2017-439



# Helicopter noise simulation and experimental technique for its validation

*Zaytsev Mikhail*, Kopiev Victor*, Vorontsov Vladimir* and Karabasov Sergey***
**Central Aerohydrodynamic Institute*
*105005, 17 Radio str., Moscow, Russia, aeroacoustics@mktsagi.ru*
***Queen Mary University of London*
*s.karabasov@qmul.ac.uk*

## Abstract
The paper presents a method of prediction the helicopter main rotor noise and the results of comparison of predictions and experimental data for hovering rotor. The noise prediction method is based on an integral representation theorem which follows from the Lighthill acoustic analogy. The nonlinear sources in the penetrable Ffowcs Williams – Hawkings (FW-H) formulation are supplied by the acoustically targeted near-field CFD computation. The near-field flow (including transonic blade tip Mach numbers) is found from the direct numerical calculation of Euler equations in the reference frame moving with helicopter blade. For validation purpose the acoustic measurements of 2 and 4-bladed model helicopter rotors have been done at outdoor rotor test rig (whirl tower) with implementation of modern data acquisition and post- processing techniques [1]. The calculated narrowband spectra showed very good agreement with experimental data in a few first harmonics of blade-pass frequency (BPF).

## 1. Introduction

Helicopters are essential part of transportation system of highly developed industrial countries and meanwhile the strong source of aviation noise. Environmental protection requirements including the protection against the adverse impact on the environment by aviation are reflected in ICAO regulations. To satisfy the ecological requirements it is necessary to predict the noise of new helicopters just at the design stage and to have reliable instrument for the development of noise reduction technologies for the existing helicopter fleet. The validated numerical code may serve as such instrument.

However, the development of numerical tool for main rotor noise prediction meets the extreme complexity of flow near the rotor blades. One method of far field aeroacoustic computation is DNS where fluid mechanics equations are solved in the whole computational domain including far acoustic field. Such direct approach is computationally intensive for obtaining a CFD solution which remains accurate in the computational domain because acoustic radiation is only ~0.01% of turbulent flow kinetic energy. In the paper we present the validation results for calculation of helicopter main rotor noise using integral method which follows from the Lighthill acoustic analogy. The non-linear sources in the penetrable Ffowcs Williams - Hawkings formulation are supplied by the acoustically targeted near-field CFD computation. This method consumes rather small computational resources then DNS and could be applied to the main rotor design practice without implementation of massive supercomputer computations.

Besides purely computational issues there is a problem of accurate validation under controlled conditions the numerical simulation of helicopter rotor acoustics. Experimental tests of the acoustic performance of model main helicopter rotors, which are the dominant source of helicopter noise, make it possible to overcome this problem. Wind tunnels (WTs) [2, 3] with an anechoic test section (e.g., DNW-LLF WT in the Netherlands) are best suited for such measurements; however, there are currently no such facilities in Russia for measuring the acoustic noise produced by large-scale model rotors in anechoic conditions. This problem is solved in part by conducting acoustic tests of model rotors in hover on an open test bench. When performing such experimental studies, it is necessary to take into account the effects of reflection from various elements of the test bench structure (e.g. concrete surface, rotor mount, fencing elements, etc.),the influence of atmospheric turbulence on the rotor noise level, etc. In view of this, our study focuses on the experimental methodology of acoustic measurements at outdoor rotor test rig (whirl tower) with implementation of modern data acquisition and post- processing techniques.

DOI: 10.13009/EUCASS2017-439



For the validation of main rotor noise predictions the acoustic measurements of model main rotors (rotor diameter D~2.7m, blade airfoil NACA23015 - NACA23012), with different flow conditions (blade tip Mach number M=0.35–0.65, blade pitch angles 0°, 4°, 8°, and 12°) were carried out at outdoor test rig with the help of microphones flush mounted on test bench floor. The post-processing of measured signals consists of averaging both in frequency and time domain and the comparison of noise narrowband spectra obtained by both methods allowed us to execute more clear separation of tonal and broadband components of helicopter main rotor noise and to compare separately the tonal noise component with numerical calculations. Comparison of experimental data on helicopter main rotor tonal noise in hover and simulation demonstrates very good agreement in the level of first few blade-pass frequency (BPF) harmonics in the wide range of investigated parameters.

## 2. Open test bench. Experimental assessment of reflections

Acoustic measurements of the noise produced by a model helicopter rotor were performed on an open test bench (Fig. 1). A specialized technique was used making it possible to quantify the signal reflected from the ground and structural elements, and post processing involved averaging in the frequency domain and simultaneous averaging in the time domain.

The test bench is a round platform with a concrete surface. A pyramidal mount with electric motors is installed at the center of the platform. These motors drive a rotor hub with the studied helicopter rotor models mounted on top. Steel box-shaped columns are arranged along the perimeter of the test bench. A metallic mesh, which prevents the dispersion of blades in the event of their failure during testing, is secured to both sides of these columns. Reinforcing elements are installed around the entire circumference of the test bench in order to strengthen the column structure.

Five 1/4" prepolarized microphones with a built-in preamplifier with a nominal sensitivity of 5 mV/Pa, and a frequency range 20–5000 Hz Brüel&Kjær (B&K)type 4935 and a 12-channel LAN-XI 3053-B-120data acquisition module were used in measurements on the open test bench. Calibration was performed with a B&K type 4228 pistonphone.

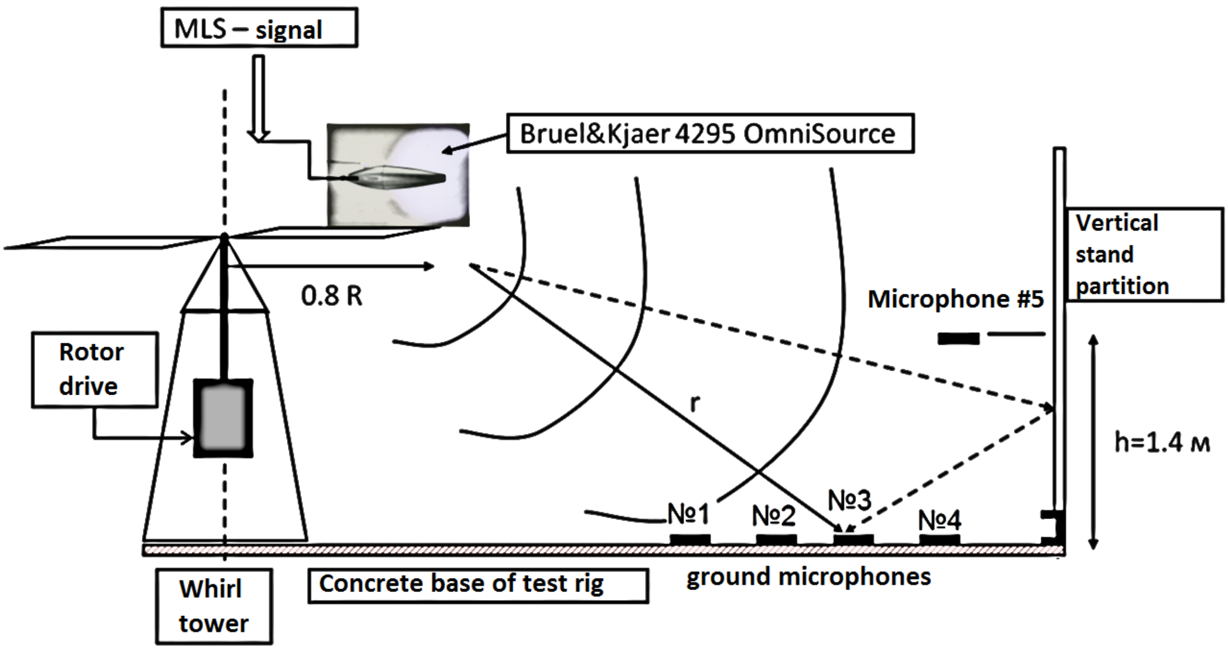


Figure 1: Scheme of open test rig for acoustic measurements of model helicopter rotor in hover

In order to quantify the signal reflection from the ground in measurements on the open test bench microphone nos. 1–4 (Fig. 1) were mounted on the concrete floor of the test bench on special square plywood boards (the area of each plywood sheet was 1 m$^2$ and the plywood thickness was 20 mm). The microphones were lying on board surface. It was demonstrated in [4] that such a microphone arrangement makes it possible to use a constant sound pressure level correction of - 6 dB for reflection from the ground in a wide frequency range from several hertz to 5 kHz in near-ground measurements. One microphone (no. 5) was mounted on a stand at a height of h= 1.4 m above the ground for comparison with the others (see Fig. 1).

In order to choose the optimal microphone configuration that minimizes the influence of reflections from test bench structural elements the Method of Maximum Length Sequences (MLS) was used. The detailed description of method

DOI: 10.13009/EUCASS2017-439



is presented in [5, 6] and in the present paper we concern only the results of MLS implementation to the model rotor measurements.
B&K type 4295 OmniSource was mounted in the rotor rotation plane (Fig. 1) at a distance of ~0.8R from the rotor axis (R is the model rotor radius). The source has monopole directivity in a wide frequency range and produced a specially synthesized signal with an autocorrelation function close to the delta function. Using this signal produced by a reference source, the two-microphone method for measuring the volume velocity, and subsequent post processing, one may obtain (using specialized processing software) the impulse response of the system. This response makes it possible to determine the reflection source, and evaluate the relative contribution of the reflected signal to the total signal recorded by the microphone at a given point.

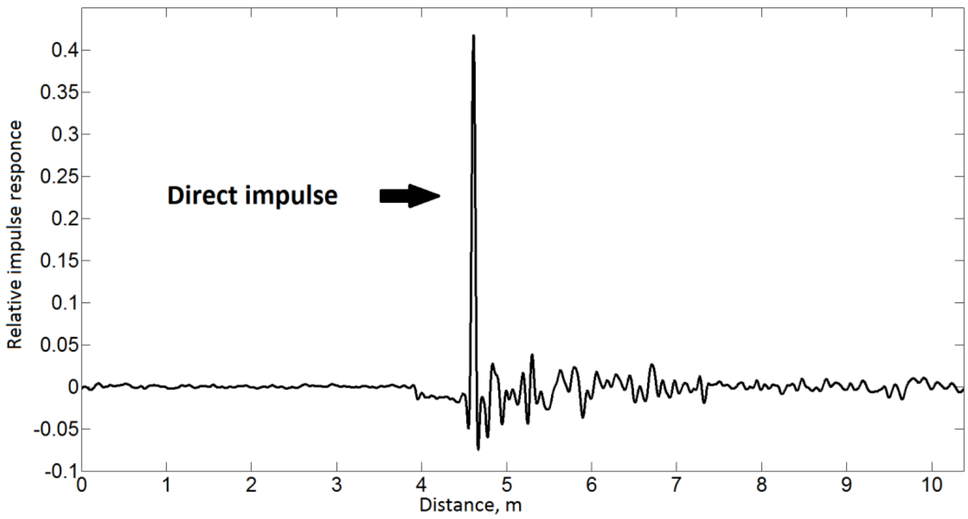


(a)

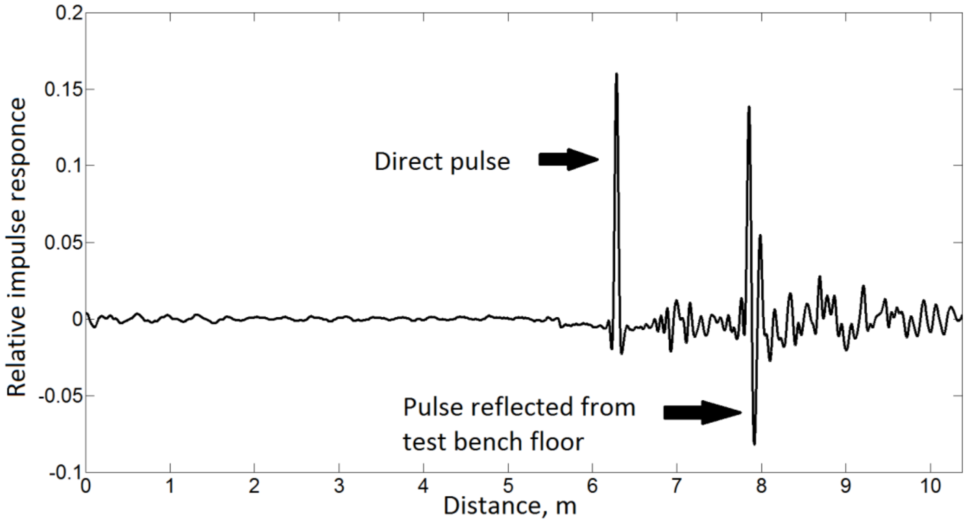


(b)

Figure 2: Relative impulse response at (a) microphone no. 1 flush mounted with the floor and (b) microphone no. 5 installed at a height of 1.4 m above ground

Figures 2a–2b show typical normalized impulse response at two microphones: flush mounted ground microphone no. 1 and microphone no.5 mounted on a stand at a height of 1.4 m above the test bench surface. The dependences in Fig. 2a reveal an almost complete lack of reflections in the signals at microphone no. 1, located the farthest from the fencing. The response at microphone no. 5 (Fig. 2b) mounted on a stand at a height of 1.4 m above the test bench surface reveals a signal reflected from the ground with an amplitude close to that of the primary signal. This usually leads to strong interference distortion in the acoustic spectrum.
Comparison of the noise spectra of the model rotor in Fig. 3 demonstrates that the interference of the direct and reflected from the test bench floor signals at microphone no. 5 considerably affects the noise levels of the first three BPF harmonics. As follows from comparison the destructive interference leads to underestimation of sound pressure levels (SPL) in low-frequency (50 – 300 Hz) and high-frequency (above 3 kHz) ranges. This influence of reflections

DOI: 10.13009/EUCASS2017-439



to the measured acoustic signal is particularly important at low frequencies, since the overall noise level in the considered rotor operation mode (four-bladed rotor with a blade pitch angle of 8°and blade tip Mach number M = 0.65) is determined primarily by the amplitudes of the lower BPF harmonics.

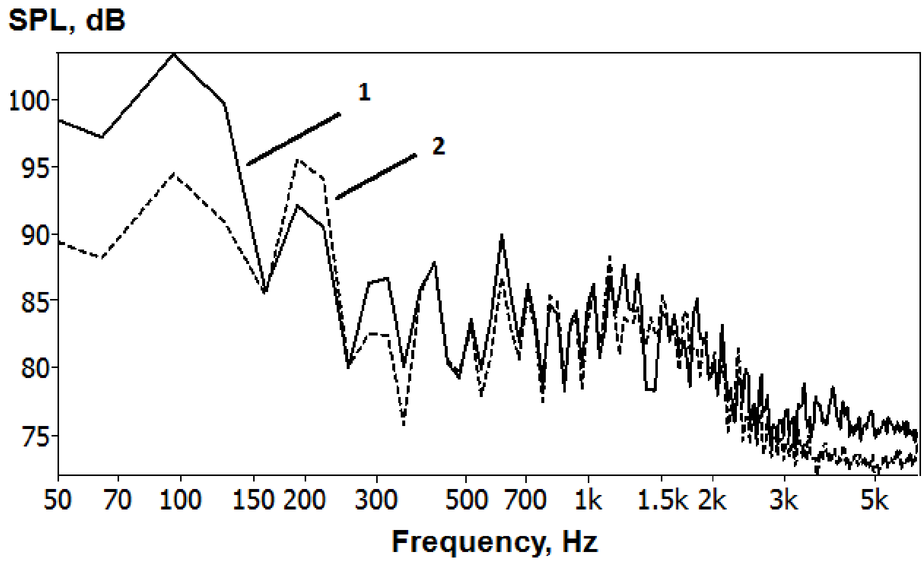


Figure 3: Sound pressure spectra measured by: (1) “ground” microphone no. 6 with correction Δ = – 6 dB and by microphone no. 5 at height of 1.4 m above ground (2).

## 3. Calculation of integral and distributed aerodynamic loading of model main rotor in hover

This article contains results of aerodynamic calculations, which present the basis for obtaining far field acoustic data. In calculation we consider the model main rotor in hover with rectangular zero-twist blades (Fig. 4) with a chord of 130 mm (constant over the span) and composed of  NACA 23012 -  NACA 23015 airfoils.

Figure 4: Plan view of model rotor blade

The main technical parameters of model rotor are as follows:

| | |
|---|---|
| Rotor diameter | D= 2.76 m. |
| Blade chord | c=130 mm. |
| Blade number | 2 or 4. |
| Solidity | σ= 0.06 or0.12. |

DOI: 10.13009/EUCASS2017-439



Blade twist Δφ= 0°.

The comparison of aerodynamic and acoustic predictions with experiment was carried out for a few representative operating conditions from available database obtained during test campaign at helicopter main rotor open test bench.

For numerical solution of three-dimensional Euler equations the structured computational grid with resolution 99×30×50 cells was used. In chordwise XY cross-sections the curvilinear O-type mesh (Fig. 5a) was implemented. For concentration of mesh lines near blade surface the polynomial node distribution method was applied. At blade tip two-dimensional grid lines were turned around OY axis, forming a hemispherical grid with axis coincided with blade tip edge.

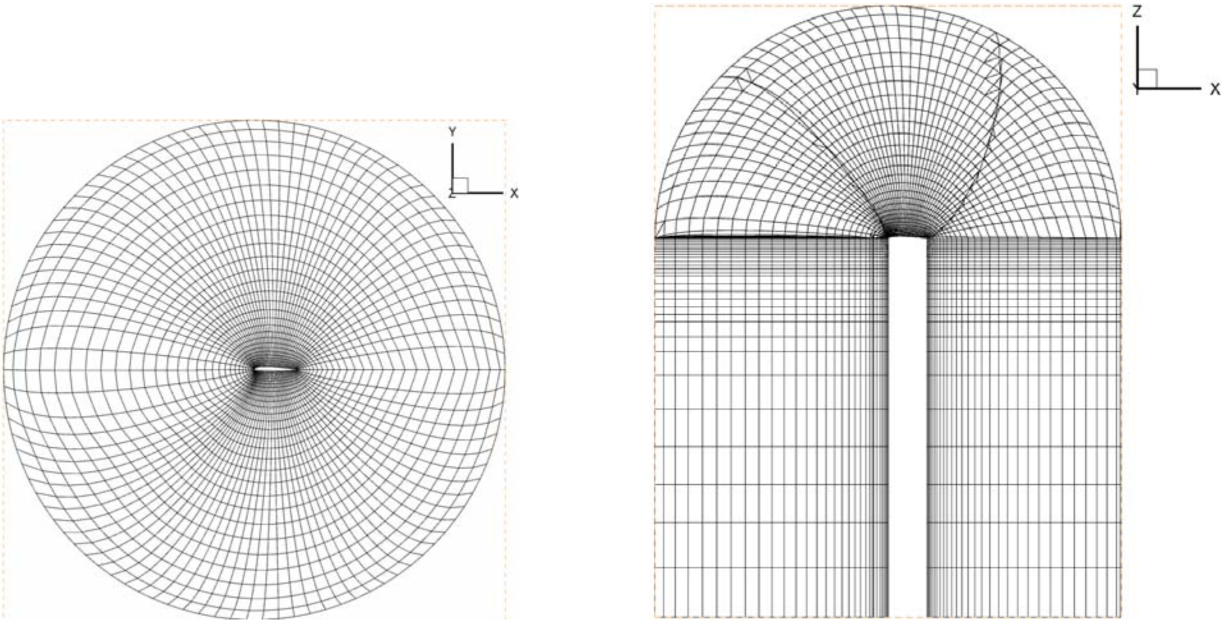


a) b)

Figure 5: – Two sections of computational grid: a) XY section, spanwise coordinate r = 0.94 R, where R – rotor radius, б) XZ plane

Near aerodynamic field is found from the direct numerical calculation of Euler equations in the reference frame moving with the helicopter blade [7]:

$$\frac{\partial U}{\partial t}+\frac{\partial F}{\partial x}+\frac{\partial G}{\partial y}+\frac{\partial W}{\partial z}=Q$$

$$U=\left(\rho,\rho u,\rho v,\rho w,\rho E\right),$$

$$F=F\left(U\right)=\left(\rho u,\rho u^2+p,\rho uv,\rho uw,u\left(\rho E+p\right)\right)^T,$$

$$G=G\left(U\right)=\left(\rho v,\rho vu,\rho v^2+p,\rho vw,v\left(\rho E+p\right)\right)^T,$$

$$W=W\left(U\right)=\left(\rho w,\rho wu,\rho wv,\rho w^2+p,w\left(\rho E+p\right)\right)^T,$$

$$Q=\left(0,q_u,q_v,q_w,\ uq_u+vq_v+wq_w\right)^T$$

where u, v, w – velocity components, $p$ , $\rho$ - pressure and density. $q_u$, $q_v$, $q_w$ – non-inertial force components.

The main angles which define blade motion are: 1) azimuthal angle ψ around rotation axis in (z, x)-plane, 2) pitching angle of rotor axis $\alpha_t = const$ in the (y,z)-plane, blade pitch angle $\varphi=\varphi\left(\psi\right)=\varphi\left(t\right)$ in (y,z)-plane.

Successive application of 2D rotation translation of coordinate system for 3D Euler equations allows to obtain components of non-inertial forces:

1) with account for rotation in (z,x)-plane

DOI: 10.13009/EUCASS2017-439



$$\begin{pmatrix} q_u \\ q_v \\ q_w \end{pmatrix} = \rho \begin{pmatrix} 2\Omega w + \Omega^2 \cdot \delta x' + \frac{d}{dt}\Omega \cdot \delta z' - \cos\psi\left(\frac{d}{dt}U_\infty\right) \\ 0 \\ -2\Omega u + \Omega^2 \cdot \delta z' - \frac{d}{dt}\Omega \cdot \delta x' + \sin\psi\left(\frac{d}{dt}U_\infty\right) \end{pmatrix},$$

$$\begin{aligned} \delta z' &= \delta z \cdot \cos\psi(t) + \delta x \cdot \sin\psi(t), \\ \delta x' &= -\delta z \cdot \sin\psi(t) + \delta x \cdot \cos\psi(t) \end{aligned} ,$$

where $\delta x = x - x_{0,}\ \delta z = z - z_0$, $and$ $(x_0 ; z_0)$ - rotor axis coordinates;

2) with account for rotation in (y,z)-plane

$$\begin{pmatrix} q_u \\ q_v \\ q_w \end{pmatrix} = \rho \begin{pmatrix} 2\Omega\, w + \Omega^2 \cdot \delta x'' + \frac{d}{dt}\Omega \cdot \delta z'' - \cos\psi\left(\frac{d}{dt}U_\infty\right)\cos\alpha_t \\ -\frac{d}{dt}U_\infty \sin\alpha_t \\ -2\Omega u + \Omega^2 \cdot \delta z'' - \frac{d}{dt}\Omega \cdot \delta x'' + \sin\psi\left(\frac{d}{dt}U_\infty\right)\cos\alpha_t \end{pmatrix}$$

$$\begin{aligned} \delta y'' &= \delta y' \cdot \cos\alpha_t + \delta z' \cdot \sin\alpha_t, \\ \delta z'' &= -\delta y' \cdot \sin\alpha_t + \delta z' \cdot \cos\alpha_t \end{aligned} ,$$

where $\delta y = y - y_0, dz = z - z_0$, $(y_0 ; z_0)$ -rotor plane center coordinates;

and 3) with account for rotation (x,y)-plane

$$\begin{pmatrix} q_u \\ q_v \\ q_w \end{pmatrix} = \rho \begin{pmatrix} -2\Omega\varphi v - \frac{d^2}{dt^2}\varphi(y - y_0) + \left(\frac{d}{dt}\varphi\right)^2 (x - x_0) + cos\varphi \cdot K + sin\varphi\left(\frac{d}{dt}U_\infty\right)\sin\alpha_t \\ 2\frac{d}{dt}\varphi u + \frac{d^2}{dt^2}\varphi(x - x_0) + \left(\frac{d}{dt}\varphi\right)^2 (y - y_0) + sin\varphi \cdot K - cos\varphi\left(\frac{d}{dt}U_\infty\right)\sin\alpha_t \\ -2\Omega \cdot A + \Omega^2 (z - z_0) - \frac{d}{dt}\Omega \cdot X - \sin\psi\left(\frac{d}{dt}U_\infty\right)\cos\alpha_t \end{pmatrix}$$

$$\begin{aligned} \delta x''' &= \delta x'' \cdot \cos\varphi(t) + \delta y'' \cdot \sin\varphi(t), \\ \delta y''' &= -\delta x'' \cdot \sin\varphi(t) + \delta y'' \cdot \cos\varphi(t) \end{aligned} ,$$

where

$$\Omega = \frac{d}{dt}\psi(t), \varphi = \varphi(\psi), U_\infty = U_\infty(t)$$

$$K = 2\Omega\, w + \Omega^2 \cdot X + \frac{d}{dt}\Omega \cdot (z - z_0) + \cos\psi\left(\frac{d}{dt}U_\infty\right)\cos\alpha_t,$$

$$A = u\cos\varphi + v\sin\varphi - \frac{d}{dt}\varphi \cdot \sin\varphi \cdot (x - x_0) + \frac{d}{dt}\varphi \cdot \cos\varphi \cdot (y - y_0),$$

$$X = \cos\varphi \cdot (x - x_0) + \sin\varphi(y - y_0)$$

and $(x_0 ; y_0)$ - blade rotation center coordinates, $z_0$ - rotor center coordinate.

Figure 6 shows the results of pressure field calculations at several sections in spanwise locations. The pressure contours demonstrate absence of distortions associated with reflections from boundaries of calculation domain and provide insight into general character of solution.

DOI: 10.13009/EUCASS2017-439



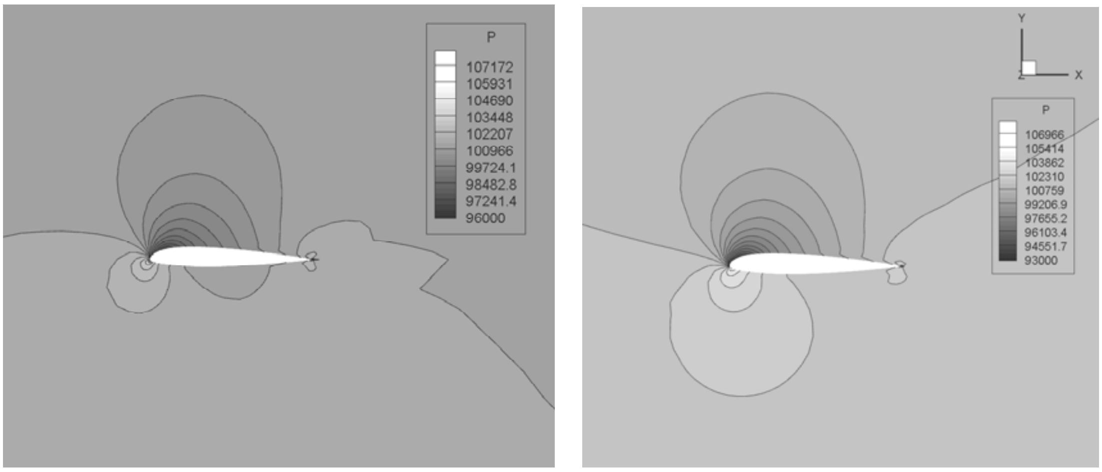


a)

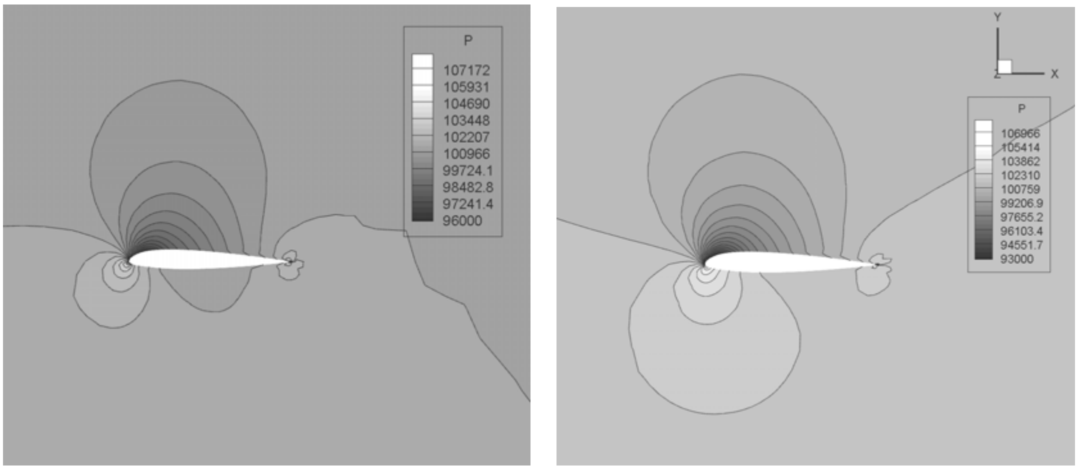


b)

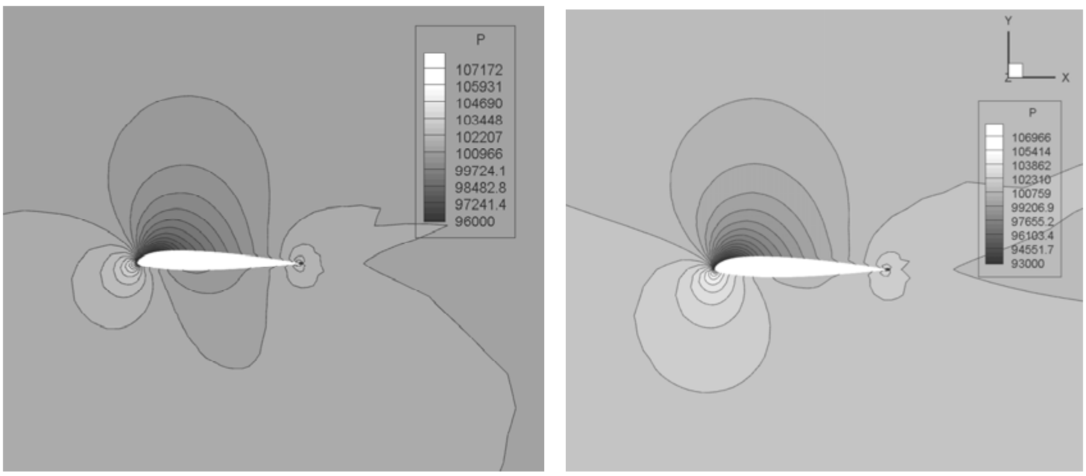


c)

Figure 6: Pressure field isolines at three spanwise locations, blade tip Mach number M = 0.35, left column – blade pitch angle φ= 4°, right column - φ= 8°: a) r = 0.7R, b) r = 0.8R, c) r = 0.94R

Both the experimental and calculated integral aerodynamic characteristics – rotor thrust and torque – are presented in Fig.7 for three blade pitch angles φ= 4°, 8° и 12°. It can be seen that the agreement between experimental results and predictions improves with increase in blade pitch angle and corresponding increase in blade loading. It can be explained by more stable performance of test rig and more reliable measurements of rotor thrust and torque for high lift regimes.

DOI: 10.13009/EUCASS2017-439



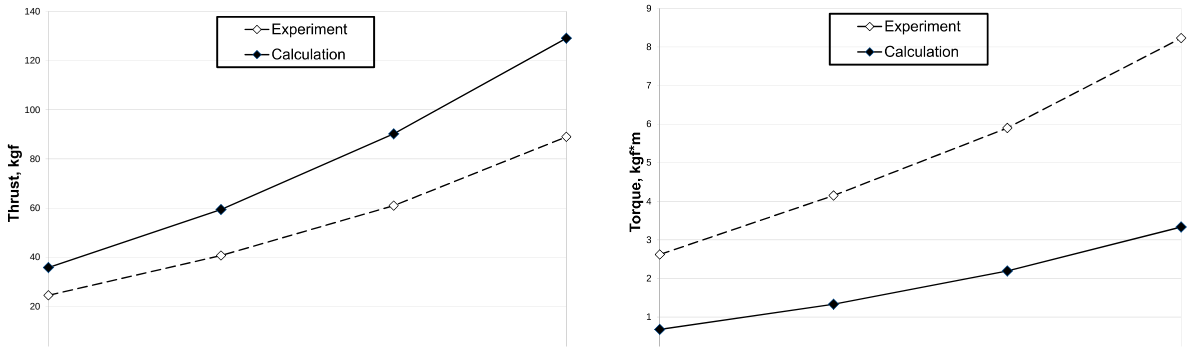


a)

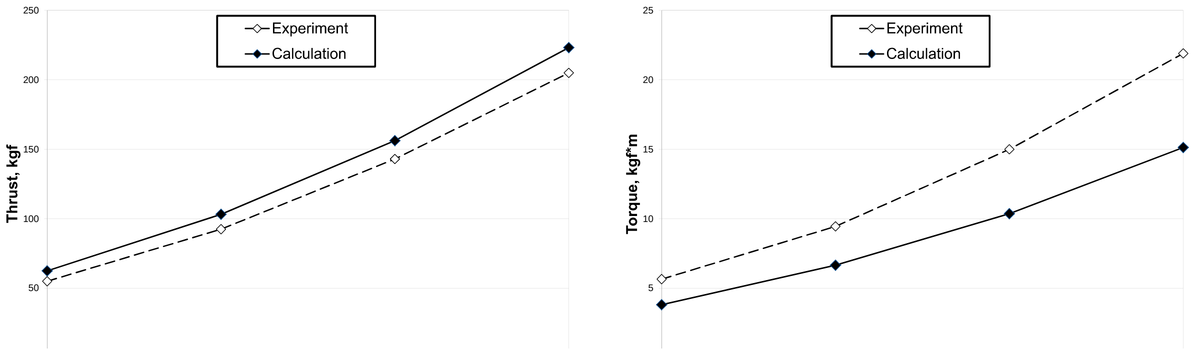


b)

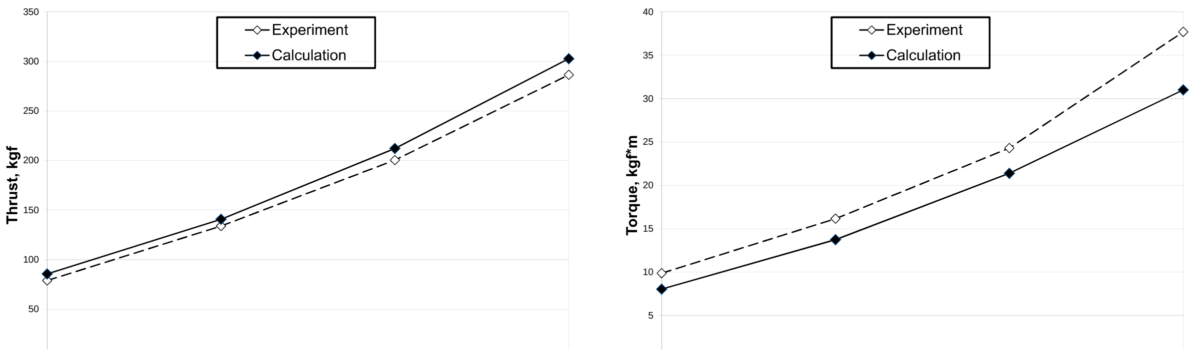


c)

Figure 7: Model rotor thrust and torque as function of blade tip Mach number: a) φ= 4°, b) φ = 8°, c) φ = 12°, two-bladed rotor.

The predicted thrust values are in very good agreement with those from experiment (the maximum relative error for the case of φ = 12° is 5.4% at blade tip Mach number M=0.65). For the torque the discrepancy between experiment and predictions is more noticeable even for large blade pitch angles. In the first place it can be explained by the fact that the Euler-based predictions doesn't take into account the viscous blade drag components that make substantial contribution to the rotor torque.

DOI: 10.13009/EUCASS2017-439



## 4. Validation of acoustic predictions for model main rotor in hover

For comparison of acoustic calculations with experiment the representative operating regimes of model helicopter main rotor in hover were chosen from the extensive database previously obtained at open test rig. Test matrix consisted in simultaneous acoustic and aerodynamic measurements of hovering model rotor. Blade tip Mach number has been varied in the range M=0.35 – 0.65. For every value of Mach number four blade pitch angles φ= 0, 4°, 8°, 12° were used.

From the results of above mentioned metrological tests (see chapter 2) the optimal microphone configuration in terms of minimizing the reflections from structural elements of test rig was defined. Microphone coordinates in rectangular reference frame with the center at rotor axis as well as the observation angle $\Theta$ between blade rotation plane and direction to microphone are presented in Table 1. The range of acceptable values of angle $\Theta$ was about ~25.

Table 1: Far field microphone coordinates

| Microphone coordinates | X, m | Y, m | Distance to microphone r, m | Θ, deg. |
|---|---|---|---|---|
| Microphone #1 | 3.9 | 4.35 | 5.8 | 48 |
| Microphone #2 | 4.9 | 4.35 | 6.5 | 42 |
| Microphone #3 | 5.9 | 4.35 | 7.3 | 36 |
| Microphone #4 | 6.9 | 4.35 | 8.2 | 32 |
| Microphone #5 | 6.9 | 2.95 | 7.5 | 23 |

Typical narrowband spectrum of helicopter main rotor noise measured during tests is shown in Figure 8.

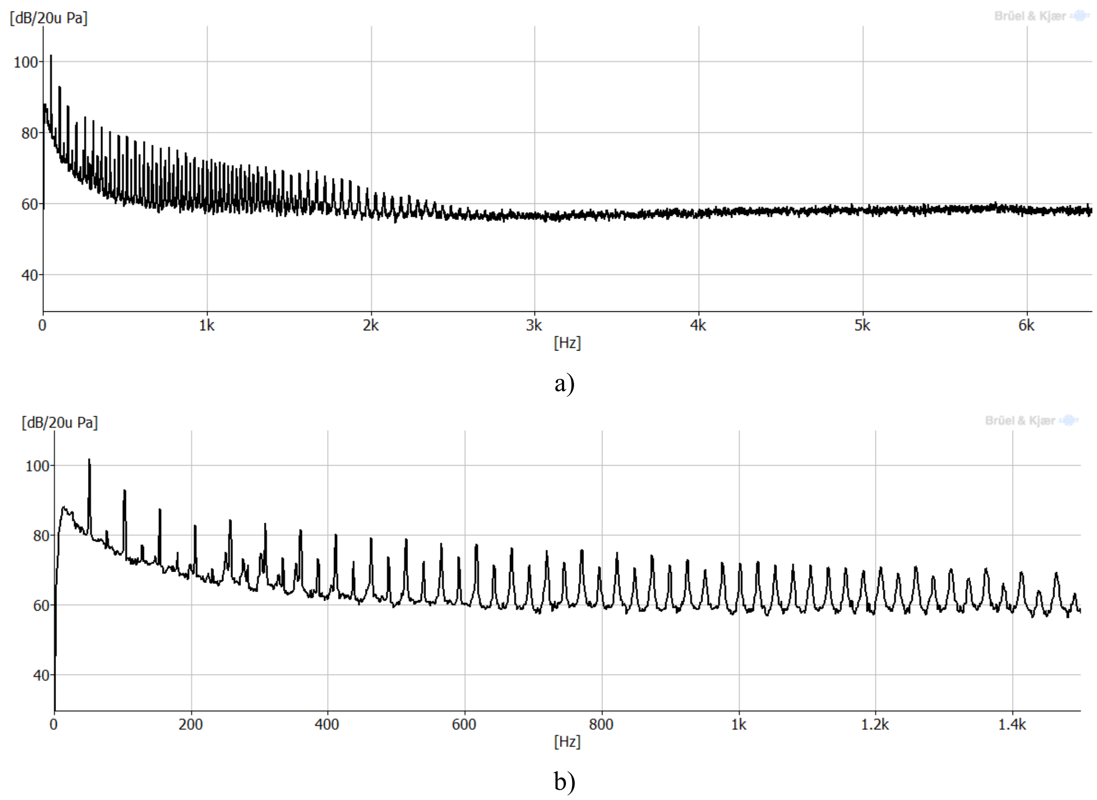


Figure 8: Narrowband spectrum of helicopter main rotor noise (2 blades), φ= 12°, M= 0.65: a) frequency range 0 – 6.4 kHz, b) low frequency range 0 – 1.5 kHz

DOI: 10.13009/EUCASS2017-439



Figure 8 shows that the overall rotor noise is substantially defined by tonal components concentrated in low- and mid-frequency spectrum domain < 2.5 kHz and having maximum amplitudes at blade-pass frequency (BPF) and a few first BPF's harmonics. Besides that the hovering rotor noise is characterized by high level of broadband noise in low frequency region (<500 Hz) due to interactions between blade and wakes from previous blade, which remain near blade rotation plane in the absence of incident flow. With increase in blade pitch angle the relative contribution of broadband noise decreases (due to increased downwash) that leads to better agreement between calculated and experimental values of rotor thrust and torque (see Fig. 7).
The spectrum presented in Figure 8 was obtained by standard method of spectral averaging with its block diagram shown in Figure 9a. For such type of signal post-processing, as shown in [8], the total spectrum of rotor noise $G_{XX} = G_{AA} + G_{MM}$ is the sum of deterministic component $G_{AA}$, associated with blade rotation, and spectrum of stochastic component $G_{MM}$.

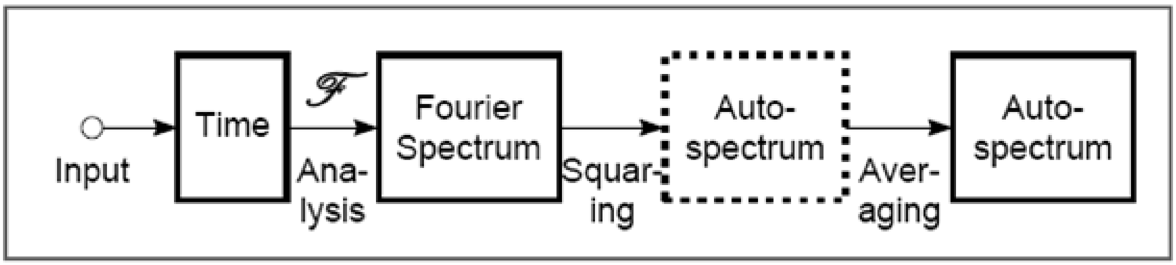


a)

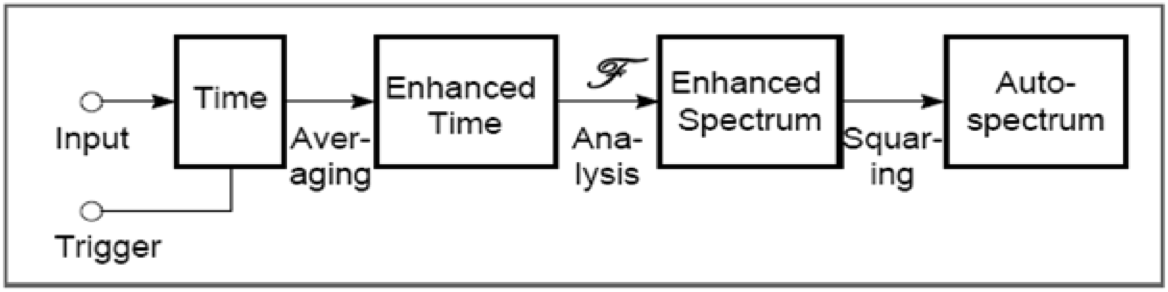


b)

Figure 9: Block diagram of: a) standard method of spectral analysis with averaging in frequency domain and b) synchronous time domain averaging [8]

However, the prediction based on Euler equations solution is principally targeted on tonal component of rotor noise and not suitable for broadband calculations. In the present paper the experimental data were therefore specially post-processed: for separation of tonal and broadband rotor noise components the method of synchronous time domain averaging was used (Fig. 9b). For such post-processing technique the total spectrum is the sum $G_{XX} = G_{AA} + 1/N\ G_{MM}$, where $G_{AA}$ deterministic component synchronous with blade rotation and $G_{MM}$ is the spectrum of non-correlating noise, N – number of averages. Thus, with increasing of averaging numbers the contribution of stochastic component $G_{MM}$ in the total spectrum decreases. Meanwhile, tonal components remain staying.

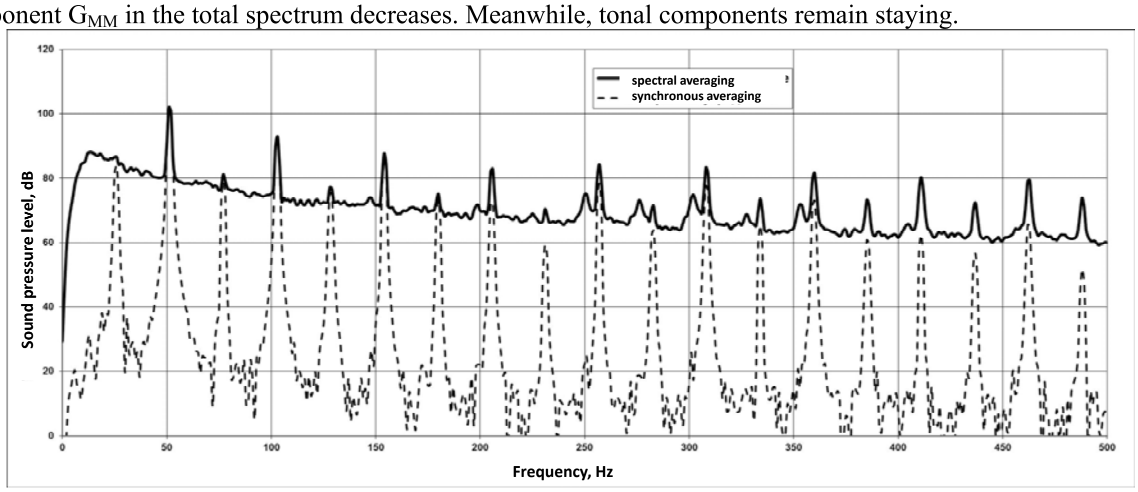


Figure 10: Comparison of total and tonal rotor noise spectra (2 blades), φ= 12°, M= 0.65

DOI: 10.13009/EUCASS2017-439



Comparison of rotor noise spectra obtained by applying both averaging methods is shown in Figure 10. The signal from revolution probe installed on rotor shaft was used for triggering averaging process in time domain. При усреднении во временной области в качестве триггерного сигнала брался сигнал с датчика оборотов, установленного на валу винта. Therefore in tonal spectrum there exist not only BPF harmonics $f_n = f_0 \cdot b \cdot n$ (where $f_0$ - rotor revolution frequency, $b$ – number of blades, n – harmonic number), but the harmonics of rotor revolution frequency $f_m = m \cdot f_0$, which appearance could be connected with small deviations in blade installation, e.g. different angular distance between blades.
Further validation of predictions was performed for tonal rotor noise processed according to the time domain averaging. Figure 11 shows typical results of comparison of the predicted tonal noise with experimental for model rotor operating in two high lift conditions.

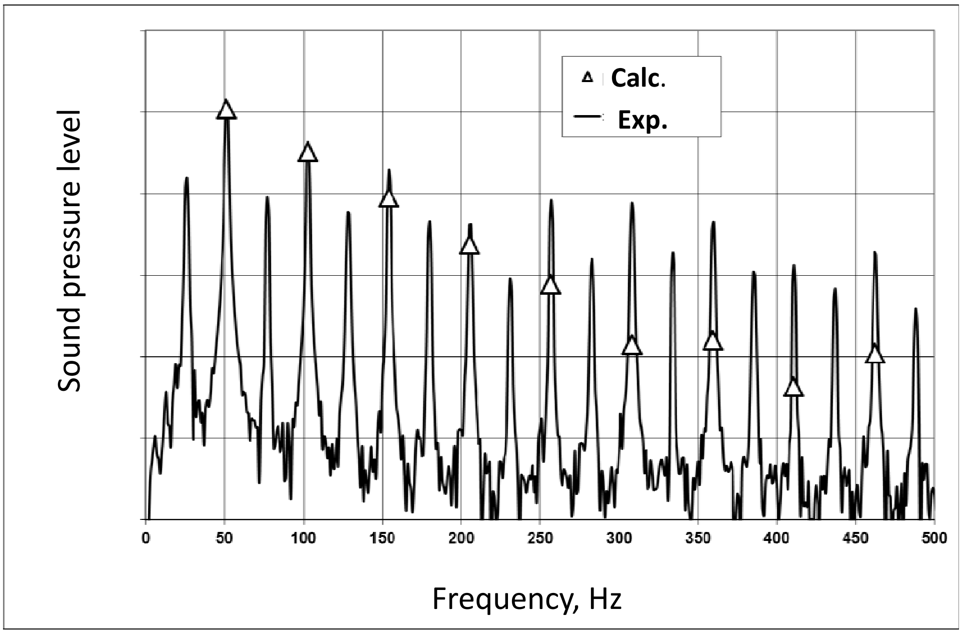


a) M= 0.65, φ= 12°

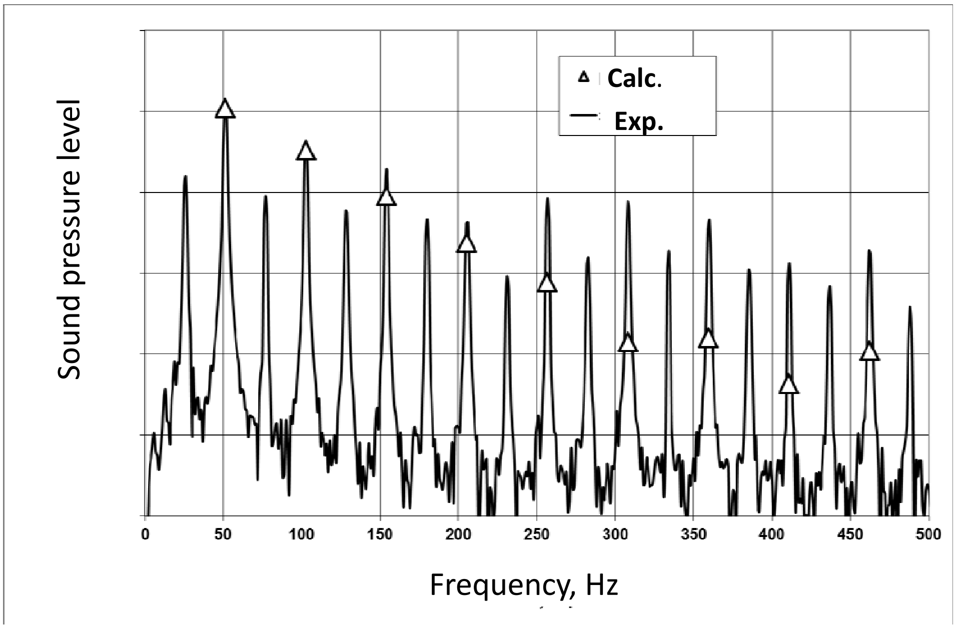


b) M= 0.55, φ= 8°

Figure 11: Comparison of calculated and experimental narrowband spectra (two-bladed roto)

DOI: 10.13009/EUCASS2017-439



## Conclusions

Analysis of validation results shows that for high lift operating conditions (large Mach number, large pitch angles) of model helicopter main rotor in hover the predicted sound pressure levels for few first BPF harmonics are in good agreement with experimental data (absolute error for 1 BPF < 1 dB). These harmonics are primarily defined by steady aerodynamic loadings of blade and contribution of non-stationary loadings for these frequencies seems to be small. With blade tip Mach number decreasing, the accuracy of prediction decreases though remaining in acceptable limits (an error ~1 – 3 dB). It seems that for low lift operating conditions the mutual influence of blades which didn't take into account in calculations leads to increasing of noise in experiment.
In whole, the comparison of experimental data on tonal noise of helicopter model rotor in hover with results of numerical simulations demonstrates good agreement in the SPL of a few first BPF harmonics. Thus, the developed numerical code gives quite good engineering estimation of maximal sound pressure level in hover without implementation of massive supercomputer calculations.

## References

[1] V.F. Kopiev, M.Yu. Zaytsev, S.L. Denisov, Vl.A. Kopiev, N.N. Ostrikov and V.A. Anikin. Experimental techniques of broadband noise eduction by examples of helicopter main rotornoise and flap side edge noise. 19th CEAS-ASC & 5th X-Noise EV Workshop on "Broadband Noise of Rotors and Airframe" 23-24 September 2015,La Rochelle, France

[2] D. A. Boxwell, F. H. Schmitz, W. R. Splettstoesser, and K. J. Schultz.1987. Helicopter model rotor-blade vortex interaction impulsive noise: scalability and parametric variations. *J. Amer. Helicopter Soc*. 32, 3.

[3] .F. H. Schmitz, E. Greenwood, R. D. Sickenberger, G. Gopalan, B. W.-C. Sim, D. A. Conner, E. Moralez and W. Decker. 2007. Measurement and characterization of helicopter noise in steady-state and maneuvering flight. Proc. 63rd Ann. Forum Amer. Helicopter Soc., Virginia Beach.

[4] William L. Willshire, Jr., and Paul A. Nystrom. 1982. Investigation of Effects of Microphone Position and Orientation on Near-Ground Noise Measurements. NASA TP 2004.

[5] V. Yu. Valyaev and A. V. Shanin. 2011. Method of Maximum Length Sequences in acoustic experiment. Acoust. Phys. vol. 57, 7, pp. 420-425,.

[6] V. F. Kop'ev, M. Yu. Zaitsev, N.N. Ostrikov, S. L. Denisov, S. Yu. Makashov,V. A. Anikin, and V. V. Gromov. 2016. On Determining the Acoustic Properties of Main Helicopter Rotor Models on an Open Test Bench. Acoust. Phys., vol. 62, 6, pp. 741–746.

[7] Karabasov S.A. 2006. Application of a hybrid approach for far-field sound prediction from high-speed helicopter blades. Mathematical Models and Computer Simulations. 18, No2, pp. 3-23.

[8] .N. Johan Wismer. "Time Domain Averaging Combined with Order Tracking" Application Note BO 0420 - 11, Brüel&Kjær.